

# Buckling driven debonding in sandwich columns

Rasmus C. Østergaard \*

*Material Research Department, Risø National Laboratory, Frederiksborgvej 399, 4000 Roskilde, Denmark*

Received 18 July 2007; received in revised form 31 August 2007

Available online 14 September 2007

---

## Abstract

A compression loaded sandwich column that contains a debond is analyzed using a geometrically non-linear finite element model. The model includes a cohesive zone along one face sheet/core interface whereby the debond can extend by interface crack growth. Two geometrical imperfections are introduced; a global imperfection of the sandwich column axis and a local imperfection of the debonded face sheet axis. The model predicts the sandwich column to be very sensitive to the initial debond length and the local face sheet imperfection. The study shows that the sensitivity to the face sheet imperfection results from two mechanisms: (a) interaction of local debond buckling and global buckling and (b) the development of a damaged zone at the debond crack tip. Based on the pronounced imperfection sensitivity, the author predicts that an experimental measurement of the strength of sandwich structures may exhibit a large scatter caused by geometrical variations between test specimens.

© 2007 Elsevier Ltd. All rights reserved.

**Keywords:** Cohesive zone modeling; Fracture; Interface crack; Delamination

---

## 1. Introduction

Sandwich structures comprising a low density core and stiff face sheets have become widely used in various engineering areas where low weight is of importance. The core primarily serves as a spacer that keeps the face sheets apart, giving the sandwich structure a high bending stiffness to weight ratio. Moreover, sandwich structures possess a high global buckling resistance when subjected to in-plane compressive loads. These properties make sandwich structures a favorable alternative in applications where weight savings are essential. Wind turbine blades (see Fig. 1), ships, aircraft structures and trains are examples where sandwich structures are used as load carrying elements (Zenkert, 1995; Thomsen, 2006; Herrmann et al., 2006).

Despite its geometrical simplicity, predicting the compressive strength of sandwich structures is complicated since many potential failure modes exist. During the last decades many studies have addressed the strength of sandwich structures. Comprehensive reviews are given in the books by Allen (1969) and Zenkert (1995). A comprehensive experimental study of the compressive strength of sandwich structures was recently conducted by Fleck and Sridhar (2002).

---

\* Tel.: +45 29857668.

E-mail address: [rasmus.c.oestergaard@risoe.dk](mailto:rasmus.c.oestergaard@risoe.dk)

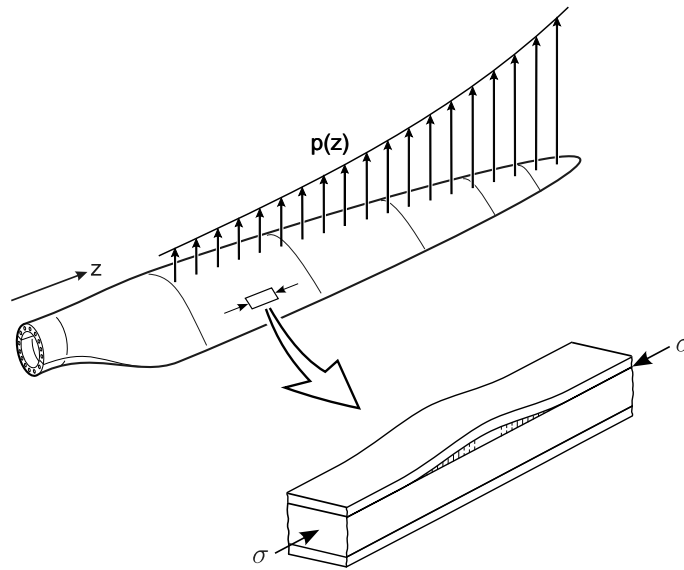


Fig. 1. Application of sandwich structures. In the wind turbine blade sandwich structures are loaded in compression on one side of the blade.

A mechanism that is important to sandwich structures is interaction of buckling modes. For a general engineering structure where more than one buckling mode (e.g., global buckling and a local buckling mode) is critical near the same external load, severe strength reduction may be experienced because the buckling modes can interact with each other. In that case, the structure may also be strongly sensitive to geometrical imperfections; especially imperfections having the same shape as the buckling modes (Van Der Neut, 1973). This is an undesired feature since even very small imperfections can reduce the strength significantly below that of the perfect structure. In sandwich structures different buckling modes can potentially interact with each other and cause a reduction of the compressive strength. Buckling mode interaction in sandwich structures has been modeled by Hunt et al. (1988) using a non-linear, six degree-of-freedom analysis. The results showed that interaction of global buckling with face sheet buckling modes results in an unstable post-buckling behavior that is sensitive to imperfections. Other studies that touch on interaction of buckling modes in sandwich structures include Kim and Sridharan (2005) and Frostig (1998).

Further complexity is added to the problem when the sandwich structure contains a debond (an area between face sheet and core with no bonding) and possible growth of this is considered. In practice, debonded areas in the face sheet/core interface are often encountered. Debonds typically result from errors in the manufacturing process or from impacts on the face sheets during use. In the presence of debonds in the interface, significant reductions of the load bearing capacity can be expected. For debonds above a critical length the strength can be limited by a complex mechanism where the debonded face sheet buckles and triggers an overall collapse. For debonds below a critical length other mechanisms can be limiting (Kwon and Yoon, 1997); for instance, global buckling, face sheet wrinkling, core shear fracture or face sheet fracture. Experimental assessments of the compressive strength of sandwich structures containing debonds are scarce, however a few studies have shown a strong influence of the extent of the debonded region (Jeelani et al., 2005; Zenkert and Shipsha, 2005; Vadakke and Carlsson, 2004). Wadee and Blackmore (2001) and Wadee (2002) extended the Hunt model (Hunt et al., 1988) and studied a sandwich structure with an initial debond that could grow according to a simple fracture mechanics model. Wadee showed that debonding may result in a highly unstable snap-back behavior that has a strong sensitivity to imperfections.

Somers et al. (1992) provides an early analysis of the load bearing capacity of partially debonded sandwich structures. Their model is based on linear elastic fracture mechanics (LEFM) and beam theory. A conclusion from their analysis is that the Euler formula for buckling of a clamped–clamped beam, with a length equal to the debond length, can be used as a first order approximation of the local debond buckling. However, recent

developments in fracture mechanics regarding composite materials have shown that LEFM is unable to describe some important phenomena in composite structures (Bao and Suo, 1992). LEFM assumes that the extent of the energy dissipating zone at the crack tip is small compared to other dimensions (e.g., laminate thickness). Many composites fail under formation of a large fracture process zone. This typically consists of a bridging mechanism such as fiber bridging. In these cases the use of LEFM is inappropriate. A comprehensive discussion of large scale bridging is given by Bao and Suo (1992).

A large scale fracture process zone can be modeled by cohesive zone modeling. Cohesive zone modeling (CZM) reaches back to Barenblatt (1959) and Dugdale (1960) but numerical implementation of the concept was pioneered by Needleman (1987). Since then CZM has become a widespread method for modeling fracture in composite structures (Hutchinson and Evans, 2000; Legarh, 2004b; Li et al., 2005; Blackman et al., 2003). CZM is a more detailed way of considering fracture since it can incorporate microscopic details of the actual fracture process taking place. In the present study, we propose a model of a partially debonded sandwich structure that is based on cohesive zone modeling.

Several experimental studies have determined interfacial fracture toughness and interface fracture mechanisms for sandwich structures (Cantwell et al., 1999; Prasad and Carlsson, 1994; Østergaard et al., 2006). Nevertheless, a full determination of the interface fracture properties in terms of cohesive law has not been done yet. Depending on processing techniques, specimen dimensions, loading and materials the debonding mechanisms change: Some sandwich structures fracture through a brittle fracture process where the crack propagates just below the interface, in the core material. Other sandwich structures fracture at the interface if this constitutes a weak plane. Yet another fracture mechanism is fiber bridging, where the crack tip propagates in an interlayer between the face sheet and core. When the crack propagates in this layer pronounced fiber bridging is seen and a large scale fracture process zone develops (Østergaard et al., 2006). This variation in the type of fracture can be modeled by CZM since both small and large process zones can be represented.

Based on the studies described above, a schematic overview of some potential failure modes relevant to the present study can be provided. Only the initiating failure mode is considered—in practice, other failure mechanisms will cause the ultimate collapse (e.g., face sheet fracture after onset of global buckling). Fig. 2 sketches equilibrium deformation-paths as axial compressive force,  $P$ , versus end-displacement,  $\Delta L$  for:

- (I) A sandwich column that buckles in the global buckling mode (without interaction with any local buckling modes). This structure has a deformation-path similar to an Euler-column, see curve I in Fig. 2. In an experimental context, such a sandwich structure will be stable in load-control (monotonically increasing load) if the load increments are sufficiently small. However, when the slope of the curve becomes horizontal equilibrium cannot be maintained because even a very small load increase will cause large deflections.
- (II) A sandwich column that collapses under buckling-interaction (e.g., interaction between the global buckling mode and face sheet wrinkling). Such a structure may exhibit an unstable behavior (Hunt et al., 1988). A typical load versus end-displacement plot is curve II in Fig. 2; after a maximum load has

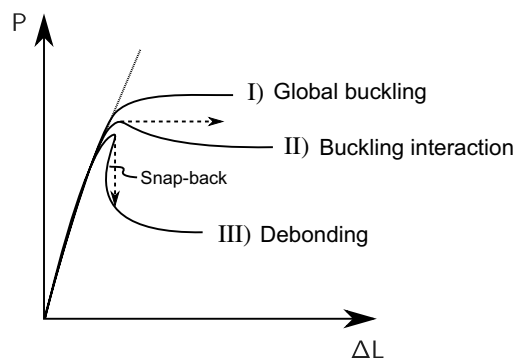


Fig. 2. Equilibrium paths for a compression loaded sandwich structure, illustrating different collapse modes.

been reached, the load decreases. In this case, load-control will result in a dynamic collapse possibly following the dashed line. However, if the loading is displacement-controlled (monotonically increasing end-displacement) the collapse will follow the equilibrium deformation-path in a stable manner.

- (III) A partially debonded sandwich structure where the debond can extend by interface fracture. As shown by Wade (2002) snap-back can occur. Consequently, unstable collapse can be expected either if the load or the end-displacement is monotonically increasing. In a practical situation where such a sandwich column is displacement-controlled, the deformation-path would follow the dashed line in an unstable manner.

The initial post-buckling path is important since this relates to imperfection sensitivity of the structure: Sandwich structures that possess a stable deformation-path (like path I in Fig. 2) are not sensitive to imperfections. In contrast, for the buckling-interaction and the debonding (path II and path III in Fig. 2) sensitivity to certain imperfections exists.

In the present study we model a compression loaded symmetric sandwich column containing a debond located at the mid-span of the column. Both face sheets and core material are taken to be isotropic. Compared to the model by Wade (2002), we apply a large strain finite element model and include a cohesive zone to model fracture. The FE method is a very adaptable method and, for later studies, other material models are easily incorporated, e.g., orthotropy of face sheets, plasticity in the core, etc. Furthermore, CZM constitutes a detailed representation of a fracture process. With the CZM we can study details of the fracture process and understand how specific types of fracture mechanisms influence the strength of partially debonded sandwich columns. The present analysis includes the effects of two simple geometrical imperfections of engineering relevance; a column axis imperfection and a local imperfection in the debonded face sheet. This will provide an understanding of how imperfections influence the strength of the sandwich column. We obtain solutions in terms of equilibrium-deformation paths.

The paper is organized as follows: First, we define the sandwich structure and introduce a number of non-dimensional parameters that uniquely specify the problem. Then, we introduce the cohesive zone to model the debonding. For the study, we select a single sandwich structure of engineering relevance. First, results are presented for the imperfection sensitivity of the partly debonded sandwich structure in a case where the interface outside the debonded region is perfectly bonded and cannot fracture. Secondly, we outline some aspects of the collapse mechanism when the debond is allowed to extend by interface crack growth. Next, the influences of interface fracture toughness and cohesive zone parameters on the post-buckling behavior is also addressed. Finally, a discussion of the results and concluding remarks are given.

## 2. Problem formulation

### 2.1. The sandwich column

In the present study we analyze a sandwich column of length  $L$ , which has face sheets with thickness  $H$  and core with thickness  $h$  (see Fig. 3). Both the face sheet material and the core material are taken to be isotropic and linearly elastic. The face material is defined by the Young's modulus  $E_f$  and the Poisson's ratio  $\nu_f$  and the core material is defined by  $E_c$  and  $\nu_c$ . In terms of non-dimensional parameters, the sandwich column is specified by

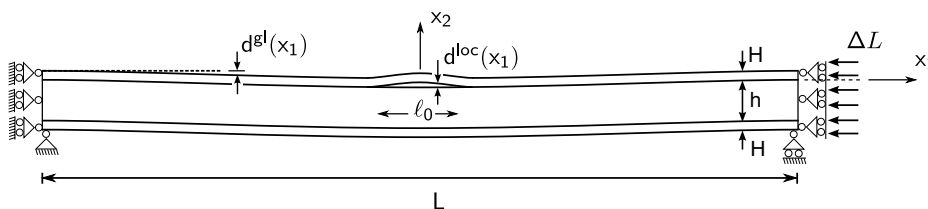


Fig. 3. Specification of the sandwich column.

$$\kappa = \frac{L}{2H+h}, \quad \eta = \frac{h}{H}, \quad \Sigma = \frac{\bar{E}_c}{\bar{E}_f}, \quad v_f \quad \text{and} \quad v_c, \quad (1)$$

where  $\bar{E} = E/(1 - \nu^2)$ .

The column contains a debonded region of length,  $\ell_0$ , located in the interval  $-\frac{1}{2}\ell_0 < x_1 < \frac{1}{2}\ell_0$ ,  $x_2 = 0$  (see Fig. 3). Along one interface ( $x_2 = 0$ ), the interface bonding is represented by a cohesive law is described in the next section.

The sandwich column has two geometrical imperfections: a global geometrical imperfection,  $d^{\text{gl}}(x_1)$ , of the column axis defined by

$$d^{\text{gl}} = d_{\text{max}}^{\text{gl}} \sin\left(\frac{2\pi x_1}{L} - \pi/2\right), \quad (2)$$

where  $d_{\text{max}}^{\text{gl}} = d^{\text{gl}}(x_1 = 0)$  is the imperfection amplitude and a local geometrical imperfection,  $d^{\text{loc}}(x_1)$  of the debonded face sheet given by

$$d^{\text{loc}} = -d_{\text{max}}^{\text{loc}} \sin\left(\frac{2\pi x_1}{\ell_0} - \pi/2\right), \quad x_1 \in \left[-\frac{\ell_0}{2}, \frac{\ell_0}{2}\right], \quad x_2 \geq 0, \quad (3)$$

where  $d_{\text{max}}^{\text{loc}} = d^{\text{loc}}(x_1 = 0)$  is the local imperfection amplitude.

The perfect beam specified by (1) now has three imperfections specified by the non-dimensional parameters:

$$\alpha = \frac{d_{\text{max}}^{\text{loc}}}{H}, \quad \beta = \frac{d_{\text{max}}^{\text{gl}}}{2H+h} \quad \text{and} \quad \xi = \frac{\ell_0}{L}. \quad (4)$$

Owing to symmetry of the problem only one-half of the column,  $x_1 \in [0, L/2]$ , is modeled; the symmetry line at  $x_1 = 0$  is fixed in the  $x_1$ -direction. Furthermore, the points  $(x_1, x_2) = (L/2, -h - H)$  and  $(x_1, x_2) = (0, -h - H)$  are fixed against displacements in the  $x_2$ -direction. At  $x_1 = L/2$  the sandwich column end is displaced by a uniform, incremental displacement in the  $x_1$ -direction. The current end-shortening is denoted  $\Delta L = -2v_1(x_1 = L/2, x_2)$ .

## 2.2. Cohesive zone model

The interface between the face sheet and core at  $x_2 = 0$  is modeled using a modified version of the Tvergaard–Hutchinson cohesive law (Tvergaard and Hutchinson, 1993), see Fig. 4. The cohesive law specifies the dependence of the tractions  $\sigma_t^I$  and  $\sigma_n^I$  on the displacements  $u_t$  and  $u_n$ . Here,  $u_n$  and  $u_t$  are the normal and tangential components of the displacement difference across the interface, while  $\sigma_n^I$  and  $\sigma_t^I$  are the corresponding normal and shear stresses in the interface (see Fig. 4b). Let  $u_n^*$  and  $u_t^*$  be characteristic values of  $u_n$  and  $u_t$  and define a non-dimensional damage zone measure as:

$$\lambda = \sqrt{\left(\frac{u_n}{u_n^*}\right)^2 + \left(\frac{u_t}{u_t^*}\right)^2}, \quad u_n \geq 0 \quad (5)$$

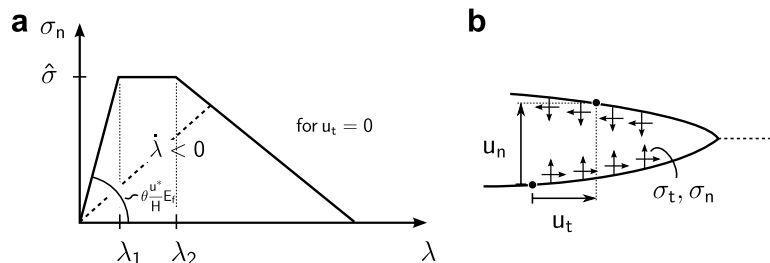


Fig. 4. (a) The normal stress component,  $\sigma_n$ , under pure normal opening. (b) Definitions of the crack face openings.

such that the tractions  $\sigma_n$  and  $\sigma_t$  drop to zero at  $\lambda = 1$ . Then, as  $\lambda$  is monotonically increasing the tractions in the interface are given by (Tvergaard, 1990):

$$\sigma_n^I = \frac{u_n/u_n^*}{\lambda} \sigma(\lambda) \quad \text{and} \quad \sigma_t^I = \frac{u_t/u_t^*}{\lambda} \frac{u_n^*}{u_t^*} \sigma(\lambda), \quad (6)$$

where  $\sigma(\lambda)$  denotes the interface normal stress under pure normal separation ( $u_t \equiv 0$ ).  $\sigma(\lambda)$  is given by a trapezoidal shape that starts at  $\sigma = 0$  at  $\lambda = 0$  and increases linearly to a peak value  $\hat{\sigma}$  at  $\lambda = \lambda_1$ . This stress level is retained until  $\lambda = \lambda_2$  where after it decreases linearly to zero. For  $0 < \lambda < 1$  this can be written as:

$$\sigma(\lambda) = \begin{cases} \hat{\sigma} \frac{\lambda}{\lambda_1} & \text{for } 0 < \lambda \leq \lambda_1 \\ \hat{\sigma} & \text{for } \lambda_1 < \lambda \leq \lambda_2, \quad \text{for } \dot{\lambda} \geq 0 \text{ and } \lambda = \lambda_{\max}, \\ \hat{\sigma} \frac{\lambda_2 - \lambda}{\lambda_2 - \lambda_1} & \text{for } \lambda_2 < \lambda < 1 \end{cases} \quad (7)$$

where  $\dot{\lambda} = \frac{\partial \lambda}{\partial u_n} \dot{u}_n + \frac{\partial \lambda}{\partial u_t} \dot{u}_t$  and  $\dot{u}_n$  and  $\dot{u}_t$  are the increments of  $u_n$  and  $u_t$ .  $\lambda_{\max}$  is the largest  $\lambda$  attained through the loading history.  $\lambda = \lambda(x_1)$  constitutes a measure of the state of the interface at  $x_1$ : For  $\lambda < \lambda_1$  the interface is undamaged. For  $\lambda_1 \leq \lambda < 1$  the interface is damaged and for  $\lambda \geq 1$  the interface has fractured.

In order to model non-monotonic opening, a linear unloading (see Fig. 4a) is used to represent the partly damaged interface:

$$\sigma_n^I = \frac{u_n}{u_n^*} \frac{\sigma(\lambda_{\max})}{\lambda_{\max}} \quad \text{and} \quad \sigma_t^I = \frac{u_t}{u_t^*} \frac{u_n^*}{u_t^*} \frac{\sigma(\lambda_{\max})}{\lambda_{\max}}, \quad \lambda < \lambda_{\max} \text{ or } \dot{\lambda} < 0. \quad (8)$$

To resist face sheet penetration of the core ( $u_n < 0$ ) we use a contact law where the normal stress is calculated according to (6)–(8), but with (6a) and (8a) replaced by

$$\sigma_n^I = k_n u_n, \quad u_n < 0, \quad (9)$$

where  $k_n$  is a stiffness constant.

The shear stresses are still given by (6) but with the dimensionless opening parameter defined as

$$\lambda = |u_t/u_t^*|, \quad u_n < 0. \quad (10)$$

In the present study we use:

$$k_n = \frac{\hat{\sigma}_n}{\lambda_1 u_n^*}. \quad (11)$$

The parameters governing the interface law are  $\hat{\sigma}$ ,  $u_n^*$ ,  $u_t^*$  together with the shape factors  $\lambda_1$  and  $\lambda_2$ . The work of separation per unit area of interface (fracture toughness),  $\Gamma$ , is given by

$$\Gamma = \frac{1}{2} \hat{\sigma} u_n^* [1 - \lambda_1 + \lambda_2]. \quad (12)$$

Equivalently the parameters can be taken as  $\Gamma$ ,  $u_n^*$ ,  $u_t^*$ ,  $\lambda_1$  and  $\lambda_2$ . In the present study we use  $u_n^* = u_t^* = u^*$ . In terms of non-dimensional constants the cohesive law is then specified by

$$\frac{\Gamma}{E_f H}, \quad \frac{u^*}{H}, \quad \lambda_1 \text{ and } \lambda_2. \quad (13)$$

The shape of this cohesive law, (7), was originally suggested to represent the fracture mechanism of ductile metals (Tvergaard and Hutchinson, 1992). Various other cohesive laws exist. For mixed mode interfacial problems (like the present) a variation of the work of separation with opening mode could be included (Chai, 2003; Tvergaard, 1990). However, for simplicity we use a fracture model that has mode mixity independent fracture toughness. This choice is also justified by the fact that the mode mixity for the present problem changes only slightly during the face sheet separation.

### 2.3. Global buckling of the sandwich column

The global buckling load  $P^{\text{gl}}$  of a sandwich column is not accurately predicted by the Euler-buckling load. A more accurate solution takes into account shear deformation of the core (Allen, 1969; Fleck and Sridhar, 2002):

$$\frac{1}{P^{\text{gl}}} = \frac{1}{P^{\text{E}}} + \frac{1}{P^{\text{S}}}, \quad (14)$$

where  $P^{\text{S}} \approx AG$ ,  $A = (h + H)^2/h$ ,  $G = E_c/(1 + 2\nu_c)$  and  $P^{\text{E}}$  is the Euler-buckling load

$$P^{\text{E}} = \frac{4\pi^2 EI}{L^2}, \quad (15)$$

where  $EI = \int_{-h-H}^H E(x_2)x_2^2 dx_2$ .

Eq. (14) gives a fairly accurate estimate of the buckling load that is in agreement with numerical results. In-depth discussions concerning global buckling of sandwich structures are found elsewhere (Bazant, 2003; Bazant and Beghini, 2004).

If we recast (14) in a dimensionless framework  $P^{\text{gl}}$  can be expressed as:

$$\frac{P^{\text{gl}}}{HE_{\text{f}}} = \frac{4\pi^2 \eta \Sigma}{\eta(\eta + 2)^2 \kappa^2 \Sigma + 4n_c \pi^2 I_0}, \quad (16)$$

where  $I_0 = (\eta^3 \Sigma + 6\eta^2 + 12\eta + 8)/12$  is a non-dimensional second moment of area and  $n_c = 2\nu_c + 1$ .

As an approximate measure of the criticality of the two buckling modes we introduce the ratio:

$$R = \frac{\epsilon_{\text{loc}}^{\text{cr}}}{\epsilon_{\text{gl}}^{\text{cr}}}, \quad (17)$$

where  $\epsilon_{\text{gl}}^{\text{cr}}$  is the average-column-strain,  $\Delta L/L$ , where global buckling initiates.  $\epsilon_{\text{loc}}^{\text{cr}}$  is an estimate of the average-column-strain,  $\Delta L/L$ , that results in buckling of the debonded face sheet.  $\epsilon_{\text{loc}}^{\text{cr}}$  is estimated from the Euler-buckling load of a clamped–clamped column with the same length as the debonded face sheet:

$$\epsilon_{\text{gl}}^{\text{cr}} = \frac{4\pi^2 \Sigma \eta / A_0}{\eta(\eta + 2)^2 \kappa^2 \Sigma + 4n_c \pi^2 I_0}, \quad (18)$$

$$\epsilon_{\text{loc}}^{\text{cr}} = \frac{\pi^2}{3(\ell_0/L)^2 \kappa^2 (2 + \eta)^2}, \quad (19)$$

where  $A_0 = \Sigma \eta + 2$ .

According to the conclusions by Somers et al. (1992),  $R < 1$  can be used as a rough criterion for predicting in which cases face sheet buckling is observable. We will compare this criterion with the numerical results obtained in this study. Eq. (17) is also used to select sandwich columns for which  $R \approx 1$  since those are of primary concern in this study.

### 2.4. Computational method

The problem defined in the previous section is solved using a large-strain finite element formulation. Eight node isoparametric elements are used. A special Rayleigh–Ritz finite element method has been used to ensure

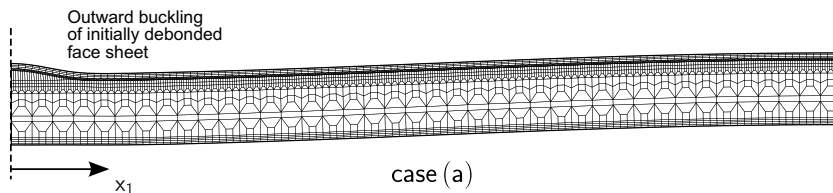


Fig. 5. The sandwich column fails by local buckling of the initially debonded face sheet when  $\alpha = 0.01$  and  $\beta = 0.01$ . The displacements are scaled  $\times 10$ .



equilibrium solutions, also in the case of snap-back (i.e., when both end-displacement increments and load increments change sign). More details concerning the computational methods can be found elsewhere (Tvergaard, 1990, 1976; Legartha, 2004a). The mesh used for the computations is shown in Fig. 5. A few calculations were carried out using more dense meshes whereby it was shown that the solutions are not mesh-dependent.

### 3. Results

#### 3.1. Model materials

In the present study we focus on a single model sandwich column that represents a sandwich structure of practical engineering interest. The stiffness parameters of the structure are defined by  $\bar{E}_f/\bar{E}_c = 100$  and  $\nu_s = \nu_c = 0.3$ . The geometry of the structure is defined by  $L/(2H + h) = 25$ ,  $\eta = h/H = 8$ . The criticality factor,  $R$ , (Eq. (17)) for a sandwich column with these parameters has been computed in Table 1 for different crack lengths. The present study will focus on cases where  $\ell_0/L \leq 0.1$  which, according to (17), is equivalent to  $R \leq 1.52$ .

Unless otherwise mentioned, the following parameters are used for the cohesive law: The fracture toughness of the interface is given by  $\Gamma = 10^{-6} E_f H$ . The critical separation in the cohesive law is  $u_n^* = u_t^* = u^* = H/10$ . The initial part of the cohesive law ( $\lambda < \lambda_1$ , see Fig. 4) gives some artificial compliance to the system, but it is a numerical necessity in cohesive zone modeling (Schellekens and De Borst, 1993). Since the interface initially has zero thickness,  $u_n$  and  $u_t$  should remain zero until the damage stress ( $\hat{\sigma}$ ) is reached and damage starts to evolve—until that point all deformation should be accommodated by the continuum around the interface. However, in many engineering problems the extra flexibility from the initial part of the cohesive law has only minor influence on the solutions. In connection to the present study, a convergence study showed that the solutions for the actual problem become practically independent the initial part of the cohesive law when the slope,  $\theta$  (see Fig. 4), fulfills

$$\theta = \frac{\hat{\sigma}}{u^* \lambda_1} \frac{H}{E_f} > 140. \quad (20)$$

Unless otherwise mentioned, the shape parameters are taken to be  $\lambda_1 = 0.01$  and  $\lambda_2 = \lambda_1 + 0.40$ . This choice of  $\lambda_1$  ensures a cohesive law that fulfills (20) and results in a solution that is practically independent of the initial part of the cohesive law.

As an example consider a sandwich column with face sheets having Young's modulus  $E_f = 70$  GPa and thickness  $H = 3$  mm. Then, the cohesive zone parameters defined above, correspond to  $\Gamma = 210$  J/m<sup>2</sup>,  $u^* = 30$   $\mu$ m and  $\hat{\sigma} = 1$  MPa (the latter is found from Eq. (12)).

#### 3.2. Imperfection sensitivity for sandwich column with perfectly bonded interface

As an introductory study, we briefly investigate the imperfection sensitivity of a partially debonded sandwich column for the case where the interface outside the debonded region is perfectly bonded. Here, perfectly bonded is defined such that the interface should not be able to open outside the debonded region, i.e.,  $u_n = u_t = 0$  for  $x_1 \notin [-\ell_0/2; \ell_0/2]$ . In practice, this is modeled by specifying the cohesive law with extremely high values of  $\Gamma$  and  $u^*$ :

$$\Gamma = 10^2 E_f H, \quad u^* = H \cdot 10^7, \quad \lambda_1 = 0.01 \quad \text{and} \quad \lambda_2 = \lambda_1 + 0.4.$$

Table 1  
The criticality factor  $R$  for different debond lengths

$\frac{\ell_0}{L}$	$R = \frac{e_{\text{cr}}^{\text{gr}}}{e_{\text{cr}}^{\text{gl}} - e_{\text{cr}}^{\text{loc}}}$
0.05	0.39
0.075	0.86
0.1	1.52
0.125	2.36



These parameters fulfill (20) so only negligible opening will occur along the interface.

The influence of  $\alpha$ ,  $\beta$  and  $\ell_0/L$  on the load-carrying capacity is shown in Fig. 6. On the vertical axis is the compressive force per unit width,  $P$ , normalized by the buckling load,  $P^{\text{gl}}$ , predicted by (14). On the horizontal axis is the column-end displacement,  $\Delta L$  normalized with the column length  $L$ . In the preceding,  $\Delta L/L$  is referred to as the average-column-strain.

Results for three different crack lengths and various combinations of imperfections are shown. We will now outline the main findings. Taking for instance the case specified with  $\ell_0/L = 0.04$ ,  $\alpha = 0.01$  and  $\beta = 10^{-5}$ , the load increases with increasing end-displacement in a linear manner until the global buckling load is reached near  $P/P^{\text{gl}} \approx 1$ . At the global buckling load a sudden transition into the post-buckling regime appears. Thereafter, continued end-displacement and buckling in the global mode takes place under constant load level (same behavior as for an Euler-column). Identical behavior is seen for a sandwich column with the same debond length and the same column axis imperfection but a larger local imperfection  $\alpha = 0.05$ . Yet another case has the same initial debond length ( $\ell_0/L = 0.04$ ) and a local imperfection  $\alpha = 0.01$  but an increased column axis imperfection,  $\beta = 0.01$ . In this case, the behavior only differs from the two previous cases in the sense that the transition into global buckling is smoother. For all three cases, mentioned above, the load reaches the global buckling load despite the presence of the debond. This can be explained by studying the openings along the debonded interface  $x_1 \in [-\ell_0/2; \ell_0/2]$ : The debonded face sheet bends inwards ( $u_n < 0$ ) and gets supported by the core (via the contact law Eq. (9)) and therefore the column practically behaves like an intact sandwich column. In a case with  $\ell_0/L = 0.04$ ,  $\beta = 10^{-5}$  and  $\alpha = 0.2$  (i.e., a larger local imperfection compared to the three previous cases) the behavior change fundamentally as a study of the openings along the debonded interface  $x_1 \in [-\ell_0/2; \ell_0/2]$  shows. For this case, the debonded face sheet buckles outwards ( $u_n > 0$ ). Furthermore, the deformation path now displays a maximum load after which the load decreases monotonically. Consequently, the column would be unstable in load-control, while under displacement control, it would exhibit a stable response.

From Fig. 6 can be concluded that the magnitude of the local imperfection,  $\alpha$ , has a large influence on whether the debonded face sheet bends inward or outward. Results not included in Fig. 6 show that the larger the column axis imperfection,  $\beta$ , the larger the local imperfection,  $\alpha$ , must be to ensure that the face sheet buckles outward.

Focusing on the influence of the initial debond length, Fig. 6 show results for three debond lengths  $\ell_0/L = 0.04$ ,  $\ell_0/L = 0.075$  and  $\ell_0/L = 0.1$ . The effect of this is strong. From  $\ell_0/L = 0.04$  to  $\ell_0/L = 0.075$  the maximum achieved load is reduced from approximately  $P/P^{\text{gl}} = 1$  to approximately  $P/P^{\text{gl}} = 0.7$ . From  $\ell_0/L = 0.075$  to  $\ell_0/L = 0.1$  the corresponding reduction is only around 0.1. The results also show that the

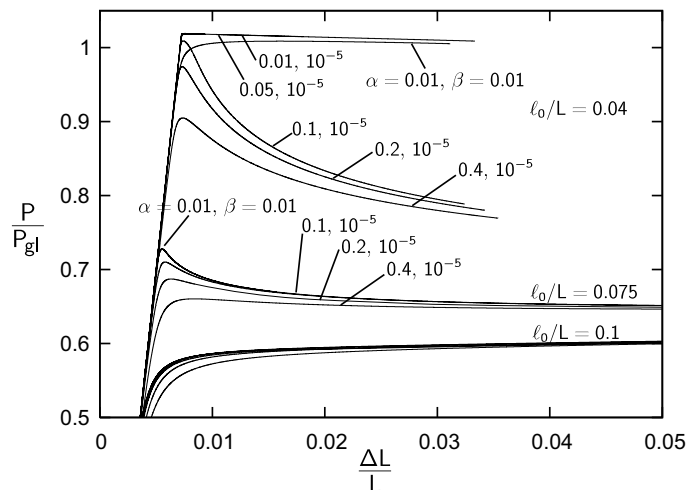


Fig. 6. Influence of the global imperfection parameter  $\beta$  and the local imperfection parameter  $\alpha$  on the compressive strength of a sandwich column with infinite fracture toughness of the interface.

curves are located closer together for longer debonds, i.e., the imperfection sensitivity decreases with increasing debond length.

### 3.3. Imperfection sensitivity—effect of debond crack growth

In this section we study the effect of imperfections on a sandwich column where the interface properties are specified according to Section 3.1:

$$\Gamma = 10^{-6} E_t H, \quad u^* = H/10, \quad \lambda_1 = 0.01 \quad \text{and} \quad \lambda_2 = \lambda_1 + 0.4.$$

For these interface parameters, the cohesive law constitutes a more realistic bonding between the face sheet and the core.

We study the influence of the three imperfections  $\ell_0/L$ ,  $\alpha$  and  $\beta$ . In the previous section, a brief, introductory, study illustrated that the sandwich column is strongly sensitive to the imperfections and that load-controlled loading of the column would result in an unstable collapse. Furthermore, it was shown that for certain combinations of the imperfections the debonded face sheet buckles outward; and for other combinations the face sheet bends inward and is supported by the core. In this section we will start off by studying two cases that result in outward buckling and inward bending of the face sheet, respectively. The two cases are specified with imperfections given by

- Case (a):  $\alpha = 0.01$ ,  $\beta = 0.01$  (outward buckling).
- Case (b):  $\alpha = 0$ ,  $\beta = 0.01$  (inward bending).

The initial debond length is chosen as  $\ell_0/L = 0.075$  for both cases.

Fig. 7 shows the response of the sandwich columns for case (a) and case (b). On the vertical axis is load,  $P/P_{gl}$  and on the horizontal axis is the average-column-strain,  $\Delta L/L$ . Initially, the force rises in a linear manner for increasing average-column-strain. When the load bearing capacity,  $P^{cr}$ , is reached both structures suffer unstable snap-back collapse.

For case (a) the collapse takes place at the same time as the debonded face sheet buckles outward and the interface fractures. Fig. 5 shows the deformed shape of the sandwich column just after the maximum load for the structure was reached. The displacements are exaggerated by a factor of 10. The post-buckling response can be divided into a number of stages as shown in Fig. 7: After the first unstable stage (1. snap-back), where

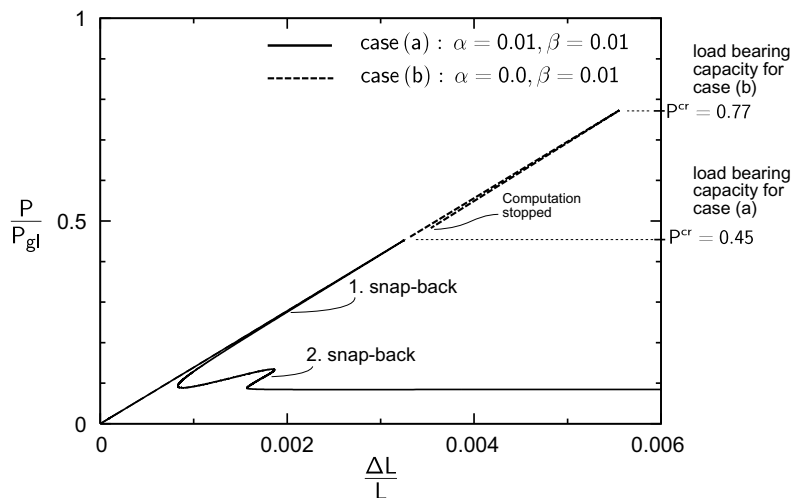


Fig. 7. Load curves resulting from two different combinations of the imperfections. In both cases the columns fail by a snap-back. The sandwich column from case (a) failed by local buckling of the face sheet and the sandwich column from case (b) failed by interface shear fracture.

debond crack growth initiates, the debond has extended to a length where a load increase is again required for increasing end-displacement. Next, a second unstable collapse (2. snap-back) causes the debond to extend to the ends of the sandwich column. The final part of the response for case (a) consists of a horizontal segment that corresponds to the buckling load of the fully debonded sandwich column.

The circumstances associated with the collapse of the sandwich column in case (b) are different: In this case, the debonded face sheet bends inwards and gets supported by the core. Therefore, the load continues to increase and the sandwich structure is compressed beyond the failure level for case (a) where the face sheet buckled outward. However, due to the geometrical imperfections, deformation in the global mode increases as the global buckling load is approached. This makes shear stresses build up in the interface and eventually interface shear fracture initiates near  $x_1 = L/4$ . At that point the maximum load (or load bearing capacity),  $P^{cr}$ , is also reached. In the following the term load bearing capacity and maximum load are used interchangeably. Hereafter the structure experiences unstable snap-back collapse as seen from the dashed line in Fig. 7 (The computation for case (b) was stopped just after the onset of crack growth). Fig. 8 shows a deformed mesh from case (b) with the displacements scaled  $\times 10$ . The load carrying capacity for the two structures are quite different; for case (a)  $P^{cr}/P^{gl} = 0.45$  and for case (b)  $P^{cr}/P^{gl} = 0.77$ . However, the results for case (b) will be sensitive to the presence of debonds located near the point where the interface shear fracture initiates ( $x_1 \approx L/4$ ). Therefore, to get a full understanding of failure mode for case (b), an additional imperfection should be included near the shear fracture initiation point. This will however not be pursued in the present paper; here we focus mainly on failure mode seen in case (a).

The transition between the failure modes in case (a) and case (b) takes place over a narrow interval of  $\alpha$  and  $\beta$ : For example, with  $\ell_0/L = 0.1$  and  $\alpha = 0.01$  the failure mode is outward buckling as in case (a) when  $\beta = 0.02$ . When increasing the column axis imperfection to  $\beta = 0.021$  the failure mode becomes as in case (b). Also, inside the window of  $\alpha$  and  $\beta$  combinations that result in outward buckling of the face sheet, a significant dependence on the values of  $\alpha$  and  $\beta$  is seen. Fig. 9 shows the load bearing capacity,  $P^{cr}$ , normalized by  $P^{gl}$  versus  $\beta$  for a range of  $\alpha$ -values and different initial crack lengths,  $\ell_0/L$ .

Taking for instance,  $\alpha = 0.01$  and  $\ell_0/L = 0.1$ , the load increases slightly in the interval  $\beta = 0$  to  $\beta = 0.021$ . In this range, failure starts by face sheet buckling and debond crack growth, a failure mode as in case (a). At  $\beta = 0.021$ , the curve displays a rapid rise of the failure load to  $P^{cr}/P^{gl} = 0.76$ . This rise reflects the shift in the failure mode to failure by global buckling and interface shear fracture (similar to case (b)). For  $\beta > 0.021$  failure mode (b) develops and for increasing  $\beta$  ( $\alpha = 0.01$  still) the failure load decreases slightly. It is noted that the curve segment corresponding to failure mode (b) is independent of the crack length and of  $\alpha$ . This is because the interface failure does not start at the initial debond.

Focusing on the failure associated with outward buckling of the face sheet (the part of the curves located to the left of the jumps in Fig. 9), the sensitivity to  $\alpha$  is pronounced; when increasing the face sheet imperfection from  $\alpha = 0.01$  to  $\alpha = 0.04$  the maximum load,  $P/P^{gl}$ , is reduced from 0.93 to 0.66 for a case with  $\ell_0/L = 0.05$  and  $\beta = 0.0035$ . This reduction is much larger than the reduction caused by the column axis imperfection  $\beta$ .

The results in Fig. 9 predict that the buckling load of a perfect column ( $\alpha \rightarrow 0, \beta \rightarrow 0$ ) is slightly higher than the buckling load,  $P^{gl}$ , predicted by (16). This may be explained by higher order effects not captured by (14); for example, as the beam is compressed the Poisson's effect increases the distance between the face sheets, this increases the stiffness and the buckling load of the column. Furthermore, including a shear correction factor (Huang and Kardomateas, 2002) may result in a more accurate prediction. For this study the observed deviation is not important.

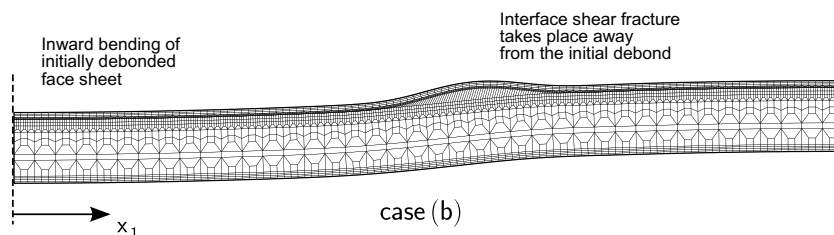


Fig. 8. When  $\alpha = 0.0$  and  $\beta = 0.01$ , the sandwich column initially deforms in a global buckling mode but an interface crack emerges due to the shear stress in the interface. The displacements are scaled  $\times 10$ .

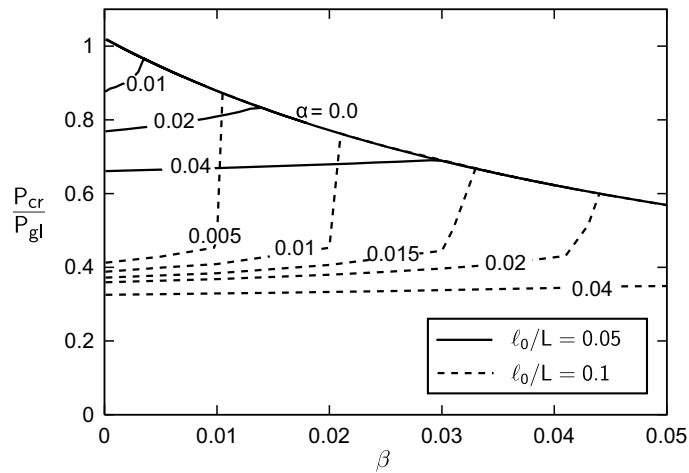


Fig. 9. Influence of the global imperfection parameter  $\beta$  and the local imperfection parameter  $\alpha$  on the compressive strength of the sandwich structure.

Another parameter that has a major influence on the load bearing capacity of the sandwich column is the initial debond length  $\ell_0/L$ . Fig. 10 shows the maximum load as a function of the initial debond length. The curves consist of a horizontal line (constant  $P/P^{gl}$ ) and a decreasing part for increasing  $\ell_0/L$ . When  $\ell_0/L$  is below a critical value (and  $\beta = 0$ ), the load reaches the horizontal line at  $P_{cr}/P^{gl} = 0.87$ , where interface shear fracture takes place as a result of the global buckling, as in case (b). For  $\ell_0/L$ -values exceeding the critical length, failure mode (a) outward buckling becomes active and the load bearing capacity is rapidly reduced for increasing  $\ell_0/L$ . The critical value of  $\ell_0/L$  is affected by the imperfections  $\alpha$  and  $\beta$  as is seen in Fig. 10: When the face sheet imperfection,  $\alpha$ , is increased the critical  $\ell_0/L$  decreases. The column axis imperfection,  $\beta$ , has the opposite effect—when this is increased the critical  $\ell_0/L$ -value also increases.

### 3.4. Detail study at the crack tip

It is of interest to investigate the behavior near the debond crack tip when the fracture process zone is modeled by a cohesive zone. Fig. 11 shows the state of the interface as the sandwich column collapses in a case (a) situation. Compressive load normalized by the global buckling load,  $P/P^{gl}$ , is on the vertical axis and the hor-

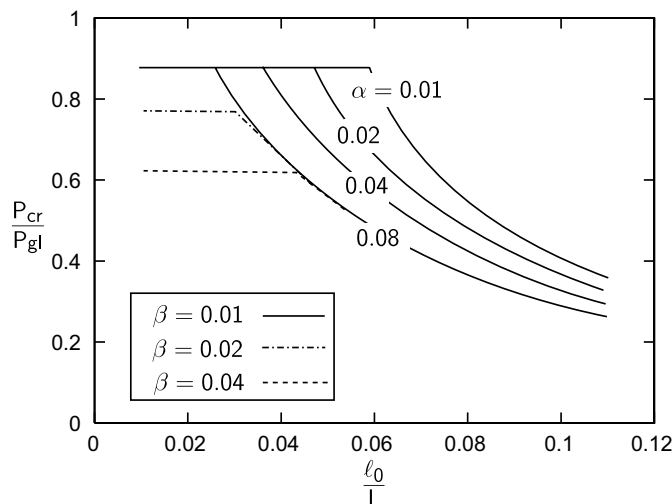


Fig. 10. Relation between crack length and maximum load the column can support.

horizontal axis shows the normalized distance to the mid-section,  $2x_1/L$ . First, focus on the solid line. This represents the correlation between the load and the location of the point in the interface at which damage is just present ( $\lambda = \lambda_1$ ); in front of this point the interface is intact ( $\lambda < \lambda_1$ ). In the initial stage of the loading, the entire interface in front of the initial debond is intact ( $\lambda < \lambda_1$ ) and no damage front is present. When the load reaches  $P/P_{gl} = 0.25$ , the cohesive element just in front of the debond crack tip ( $x_1 = \ell_0/2$ ) starts to develop damage ( $\lambda \geq \lambda_1$ ); therefore, the solid line emerges at  $x_1 = \ell_0/2$ . As the loading continues the damage front extends forward. At  $P/P_{gl} = 0.45$  the load reaches a maximum and starts to decrease while the damage front still continues to move forward. Now focus on the thin dashed line that shows the location of the crack front ( $\lambda = 1$ ). When the load has decreased to  $P/P_{gl} = 0.38$ ,  $\lambda = 1$  at the initial crack tip, so that the debond crack tip starts to propagate. The horizontal distance between the solid line and the dashed line represents the current length of the damage zone  $\ell_{DZ}$ . For example, in Fig. 11, the length of the damage zone is  $\ell_{DZ} \approx 7H$  at the onset of crack growth and it remains approximately constant in size throughout the collapse. From Fig. 11 it is also seen that throughout the process the damage front and the crack tip propagate continuously forward.

Figs. 9 and 10 have shown that the  $P - \Delta L$  relationship is significantly influenced by the local imperfection  $\alpha$ . The dependence on the imperfection amplitude  $\alpha$  may be attributed to the crack growth mechanism and the development of a damage zone prior to collapse. In order to clarify this we study how  $\alpha$  influences what occurs at the crack tip.

In Fig. 12 the horizontal axis is the position of the damage front,  $x_1/H$ , and the vertical axis is the load,  $P/P_{gl}$ . The lines represent the location of the damage front ( $\lambda = \lambda_1$ ) for different values of  $\alpha$ . Taking for instance  $\alpha = 0.02$  the damage front starts to form at the debond crack tip at  $x_1/H = 18.75$  when  $P/P_{gl} = 0.175$ . The damage front then moves forward and when it is at  $x_1/H = 26$  the maximum load is reached and the load starts to decrease. The results show that, for increasing face sheet imperfection,  $\alpha$ , the length of the damage zone at the maximum load,  $\ell_{DZ}$ , increases. At the same time the maximum load the column can carry decreases. A physical explanation of this behavior is now proposed. Initially, the debonded face sheet acts as an imperfect strut that has some rotational flexibility at its ends,  $x_1 = \pm \ell_0/2$ . Since the interface is very rigid, the rotational flexibility at the ends results mainly from flexibility of the core. However, as the sandwich column is loaded, the debonded face sheet bends outward and the interface tractions increase. Eventually, the peak stress,  $\hat{\sigma}$ , is reached and a damage zone starts to develop from the debond crack tip. The damaged zone is softer and adds extra rotational flexibility at the ends of the debond. This makes the face sheet deform like an effectively longer strut and the buckling of it takes place at a lower load.

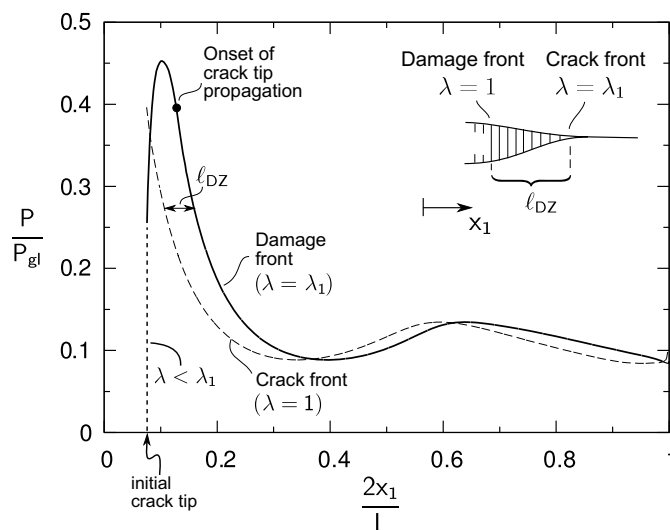


Fig. 11. Location of the damage front ( $\lambda = \lambda_1$ ) along the interface is given by the solid line. Location of the crack front ( $\lambda = 1$ ) is given by the dashed line.

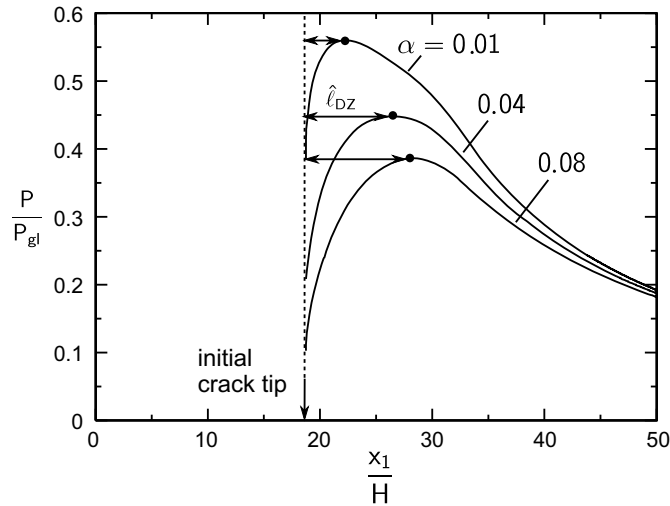


Fig. 12. Influence of  $\alpha$  on the damage zone developing at the debond crack tip.

### 3.5. Influence of the non-dimensional interface fracture toughness on the overall response

The results in the previous section have shown how the debond growth results in a structure that is very sensitive to imperfections and collapses by a snap-back mechanism. In this section we investigate how the highly unstable collapse behavior of the sandwich column (illustrated in Fig. 7) is influenced by the non-dimensional interface fracture toughness,  $\Gamma/E_f H$ . The imperfections are as in case (a), i.e.,  $\alpha = \beta = 0.01$ .

The non-dimensional interface fracture toughness is modified by changing the critical opening  $u^*$  and the peak stress  $\hat{\sigma}$  proportionally, see Fig. 13a. For instance, to accommodate a factor  $\phi$  increase of  $\Gamma/E_f H$  the parameters  $\hat{\sigma}$  and  $u^*$  are both increased by a factor  $\sqrt{\phi}$ . Figs. 14–16 show the normalized compressive load,  $P/P_{gl}$ , against  $\Delta L/L$ , for different non-dimensional interface fracture toughness values and different initial debond lengths. Results for values of  $\Gamma/E_f H$  ranging from  $10^{-6}$  to  $\infty$  are shown in the figures.

The example in Fig. 7 illustrated that the collapse comprised two snap-backs. The present results (Figs. 14–16) show that increasing the values of the non-dimensional interface fracture toughness raise the post-buckling response and ultimately it reaches a limit defined by a curve for  $\Gamma/E_f H \rightarrow \infty$ . Along with this tendency, increasing  $\Gamma/E_f H$  also changes the characteristics of the first snap-back. Taking for instance  $\ell_0/L = 0.05$  (Fig. 14), we see that as the fracture toughness is increased the slope of the curve right after the maximum load is changed. Thus, the slope is negative for  $\Gamma/(E_f H \cdot 10^{-6}) > 1000$ . From a practical point-of-view this implies that the structure is stable under prescribed displacement. Taking instead  $\ell_0/L = 0.1$  (Fig. 16), we see that while  $\Gamma/(E_f H \cdot 10^{-6}) = 20$  results in a snap-back, the snap-back has disappeared for

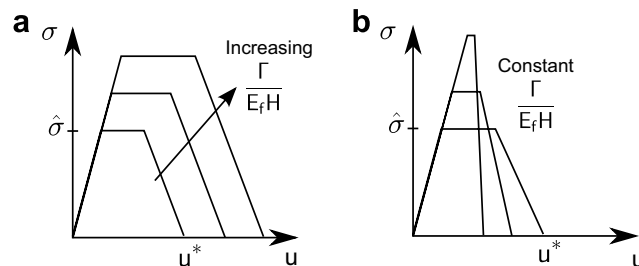


Fig. 13. Modification of the cohesive law for the parameter studies: (a) The work of separation is modified by varying the critical separation,  $u^*$ , and the maximum cohesive stress  $\hat{\sigma}$  proportionally. (b)  $\hat{\sigma}$  and  $u^*$  are varied inversely proportional so the work of separation is kept constant.

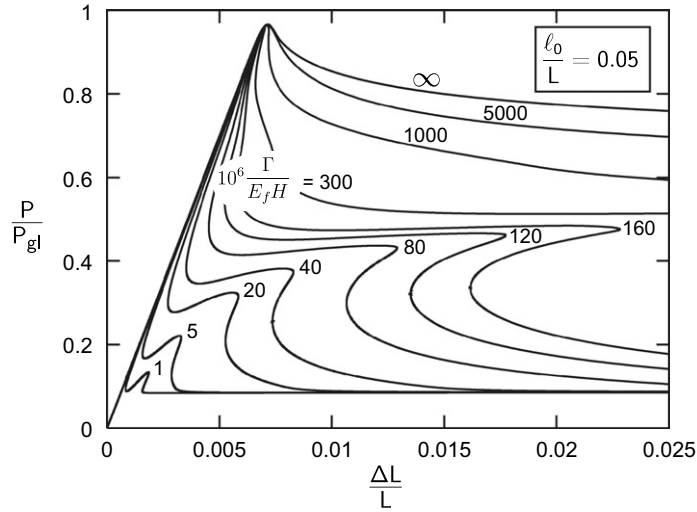


Fig. 14. Response of a sandwich column with a debond of length  $\ell_0/L = 0.05$  and different interface fracture toughness values.

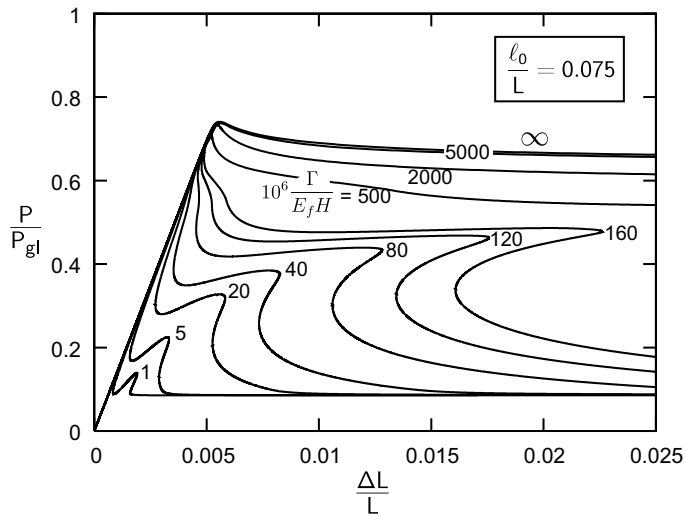


Fig. 15. Response of a sandwich column with a debond of length  $\ell_0/L = 0.075$  and different interface fracture toughness values.

$\Gamma/(E_f H \cdot 10^{-6}) = 80$ . These two examples show the general trend that the longer the debond is, the less interface fracture toughness is needed to ensure that it is stable under displacement-control.

The non-dimensional interface fracture toughness also influences the occurrence of a second snap-back. For instance, in Fig. 15, the sandwich column with  $\Gamma/E_f H = 10^{-6}$  experienced the second snap-back at  $\Delta L/L = 0.0018$  whereas an interface with  $\Gamma/(E_f H) = 40 \times 10^{-6}$  increases this value to  $\Delta L/L = 0.008$  which also is larger than the strain level at which the first snap-back sets in ( $\Delta L/L = 0.005$ ).

### 3.6. Influence of the peak stress and the critical separation of the interface

In Figs. 14–16 the increase of the interface fracture toughness was accommodated by a proportional increase of the interface parameters. In the present section the response of the sandwich column is computed with different combinations of the critical separation,  $u^*$ , (see Eq. (5)) and  $\hat{\sigma}$  while  $\Gamma/E_f H$  is maintained at a fixed value, see Fig. 13b. This way of varying the cohesive law represents the effect of changing the type of



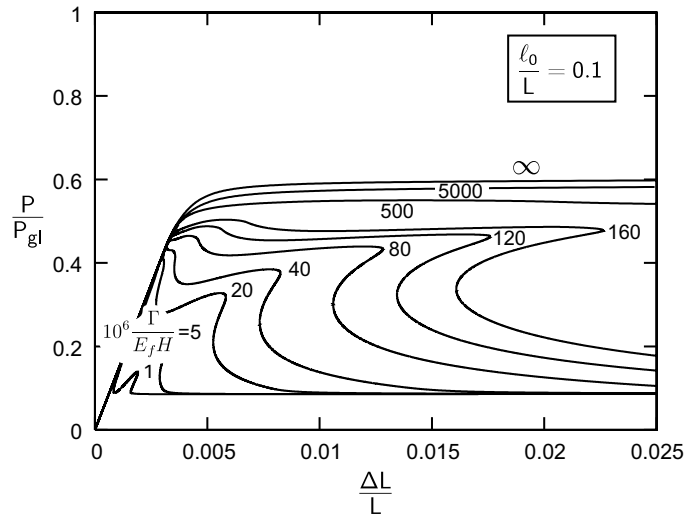


Fig. 16. Response of a sandwich column with a debond of length  $\ell_0/L = 0.1$  and different interface fracture toughness values.

fracture mechanism. The actual shape of the cohesive law may also have an appreciable effect on the response (see for instance [Chai, 2003](#), who showed that the strength of a panel with a central hole depends somewhat on the actual shape of the cohesive law). For this study,  $\Gamma/(E_f H \times 10^{-6}) = 40$  is selected to represent the interface fracture toughness and the initial debond is selected as  $\ell_0/L = 0.075$ . The results are shown in [Fig. 17](#) for values of  $u^*$  ranging from  $0.1H$  to  $2.5H$ . According to (12) each  $u^*$  corresponds to one  $\hat{\sigma}$ , see [Table 2](#).

The results show that the load carrying capacity increases as  $u^*$  decreases (and  $\hat{\sigma}$  increases). This trend may be explained as follows: As described in [Section 3.4](#) the finite deflection of the debonded face sheet prior to its buckling, causes interface stresses to build up at the debond crack tip. When these stresses reach the peak stress a softened damage zone starts to develop in front of the crack tip. This zone provides extra rotational flexibility and the debond buckling is pushed forward. However, when the interface peak stress,  $\hat{\sigma}$ , is increased, a larger finite deflection is needed to initiate damage at the crack tip and therefore the sandwich structure fails at a higher external load level, despite the fact that the fracture toughness is unchanged.

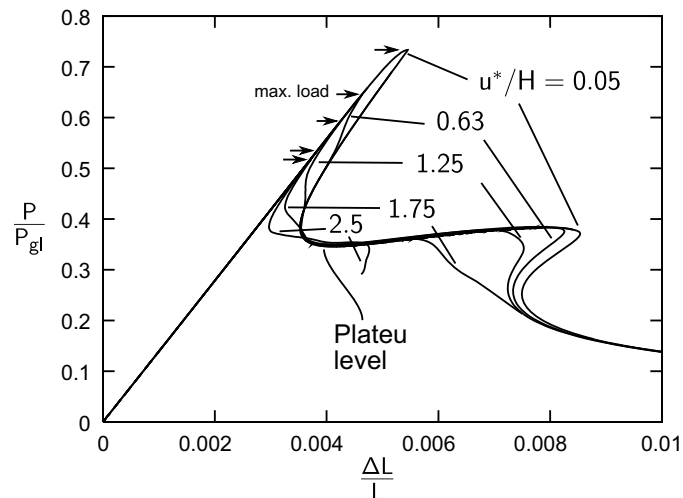


Fig. 17. The response of a sandwich column with an interface fracture toughness of  $\Gamma/(HE_f \times 10^{-6}) = 40$ . The curves represent different combinations of  $\hat{\sigma}$  and  $u^*$ . Each  $u^*$  corresponds to one  $\hat{\sigma}$ , see [Table 2](#). The maximum loads achieved are indicated by the arrows.

Table 2

Combinations of  $u^*/H$  and  $\hat{\sigma}/E_f$  that together with  $\lambda_1 = 0.01$  and  $\lambda_2 = 0.41$  provide an interface toughness value  $\Gamma/HE_f = 40 \times 10^{-6}$

$u^*/H$	$\hat{\sigma}/E_f$
0.05	$14 \times 10^{-4}$
0.63	$0.91 \times 10^{-4}$
1.25	$0.46 \times 10^{-4}$
1.75	$0.33 \times 10^{-4}$
2.5	$0.23 \times 10^{-4}$

Fig. 17 also shows that after the 1st snap-back, all curves coincide at a plateau level that is independent of the actual combination of  $u^*$  and  $\hat{\sigma}$ . However, continued compression of the sandwich column causes the curves to branch off depending on the actual combinations of  $u^*$  and  $\hat{\sigma}$ . Furthermore, the results show that the 2nd snap-back occurs at higher strains as  $u^*$  is decreased (or as  $\hat{\sigma}$  is increased).

#### 4. Discussion and concluding remarks

This study considered the influence of a global column axis imperfection and a local face sheet imperfection on the compressive strength of a sandwich column containing an initial debond. The results show a strong dependence on the imperfections: The actual combination of the imperfections controls whether the debonded face sheet bends inward and is supported by the core or if it buckles outward and triggers an overall collapse. The type of failure mode selected has a major influence on the load bearing capacity of a sandwich structure. In the case of inward bending, the face sheet does not buckle and the load continues to increase until another failure mechanism limits the load bearing capacity. In the case of a perfectly bonded interface, that limiting mechanism is global buckling. If the interface is able to fracture, the model predicts that interface shear fracture limits the load bearing capacity. However, for a true sandwich structure other failure mechanisms may limit the load bearing capacity, e.g., shear failure in the core, or yielding in the core. Also the face sheet may fail because the compressive strength or the yield stress is exceeded.

Indeed, the amplitude of the face sheet imperfection,  $\alpha$ , has a strong influence on the load bearing capacity for the cases where the column fails by outward buckling of the debonded face sheet. For instance, for a debond length  $\ell_0/L = 0.05$  and global imperfection  $\beta = 0.0035$  the onset of failure is reduced from 93% to 66% of the global buckling load when the face sheet imperfection is increased from  $\alpha = 0.01$  to  $\alpha = 0.04$ . For a real sandwich column having a face sheet thickness  $H = 3$  mm the difference between these values corresponds to no more than 90  $\mu\text{m}$ . Face sheet irregularities of this order of magnitude are commonly encountered. When fiber reinforced polymers are used as face sheets a slightly unsymmetrical layup may have imperfections of this magnitude or larger and would seem perfect prior to loading.

A physical explanation of the imperfection sensitivity was sought. A detailed study at the crack tip showed how a damage zone develops from the debonded crack tip during loading of the sandwich column. The crack tip damage zone corresponds to an effectively longer debond and therefore the debonded face sheet reaches its buckling load at a lower load, viz. the sandwich column fails at a lower load. The magnitude of the face sheet imperfection has a significant effect on the extent of the crack tip damage zone and consequently also on the buckling load of the debonded face sheet and the failure load of the sandwich column.

It is not possible to conclude that imperfection sensitivity is only introduced through the damage zone development. As shown in Section 3.2 severe imperfection sensitivity is also present even if the interface is perfectly bonded. That was interpreted as interaction of buckling modes. In a general case, imperfection sensitivity may result from a complex interplay of buckling mode interaction and development of damage at the debond crack tip.

In an experimental context, the imperfection sensitivity implies that severe scatter of the load bearing capacity can be expected. Other structures that are very sensitive to imperfections such as circular cylindrical shells also exhibit large experimental scatter. For these structures, the imperfection sensitivity has led to the practice of using a knock-down factor for the strength to achieve more useful engineering predictions of strength (Brush and Almroth, 1975).

The properties of the interface (the cohesive zone parameters) clearly has an influence on the overall collapse response of sandwich structures. To understand the influence in greater detail, we investigated the effect of interface toughness on the collapse mechanism. Generally, increasing the interface toughness was shown to have a stabilizing effect on the collapse. In some cases, increasing the (non-dimensional) interface fracture toughness changed the snap-back into a stable collapse, where both load and strain are monotonically increasing. This was seen for the longest crack lengths analyzed,  $\ell_0/L = 0.1$ , in Fig. 16. For the shorter crack lengths ( $\ell_0/L = 0.075$  and  $\ell_0/L = 0.05$ , Figs. 14 and 15) increasing the interface toughness can change the snap-back curve into an unstable curve that displays a continuously increasing end-displacement but a decreasing load during the collapse. The curves in Figs. 14–16 show that as the initial crack length is increased a lower (non-dimensional) interface fracture toughness is required to avoid the 1st snap-back.

## Acknowledgments

The author wish to acknowledge Prof. Viggo Tvergaard and Dr. Lars P. Mikkelsen for inspiring discussions. The work was supported by the Frame Work Programme “Interface Design of Composite Materials” (Danish Research Council (STVF)), Grant No. 26-03-0160.

## References

- Allen, H., 1969. Analysis and Design of Structural Sandwich Panels. Robert Maxwell M.C., M.P., London.
- Bao, G., Suo, Z., 1992. Remarks on crack bridging concepts. *Applied Mechanics Review* 45 (8), 355–366.
- Barenblatt, G., 1959. Equilibrium cracks formed during brittle fracture rectilinear cracks in plane plates. *Journal of Applied Mathematics and Mechanics* 23 (4), 1009–1029.
- Bazant, Z., Beghini, A., 2004. Sandwich buckling formulas and applicability of standard computational algorithm for finite strain. *Composites Part B: Engineering* 35 (6–8), 573–581.
- Bazant, Z., 2003. Shear buckling of sandwich, fiber composite and lattice columns, bearings, and helical springs: paradox resolved. *Journal of Applied Mechanics, Transactions ASME* 70 (1), 75–83.
- Blackman, B., Hadavinia, H., Kinloch, A., Williams, J., 2003. The use of a cohesive zone model to study the fracture of fibre composites and adhesively-bonded joints. *International Journal of Fracture* 119 (1), 25–46.
- Brush, D., Almroth, B., 1975. Buckling of Bars, Plates, and Shells. McGraw-Hill Book Company, New York.
- Cantwell, W., Scudamore, R., Ratcliffe, J., Davies, P., 1999. Interfacial fracture in sandwich laminates. *Composites Science and Technology* 59 (14), 2079–2085.
- Chai, H., 2003. Interfacial mixed-mode fracture of adhesive bonds undergoing large deformation. *International Journal of Solids and Structures* 40 (22), 6023–6042.
- Dugdale, D., 1960. Yielding of steel sheets containing slits. *Journal of the Mechanics and Physics of Solids* 8 (2), 100–104.
- Fleck, N., Sridhar, I., 2002. End compression of sandwich columns. *Composites Part A: Applied Science and Manufacturing (Incorporating Composites and Composites Manufacturing)* 33 (3), 353–359.
- Frostig, Y., 1998. Buckling of sandwich panels with a flexible core-high-order theory. *International Journal of Solids and Structures* 35 (3–4), 183–204.
- Herrmann, A.S., Zahlen, C.Z., Zuady, I., 2006. Sandwich structures technology in commercial aviation—present applications and future trend. In: *Sandwich Structures 7: Advancing with Sandwich Structures and Materials*. Aalborg University, pp. 13–26.
- Huang, H., Kardomateas, G., 2002. Buckling and initial postbuckling behavior of sandwich beams including transverse shear. *AIAA Journal* 40 (11), 2331–2335.
- Hunt, G.W., Da Silva, L.S., Manzocchi, G.M.E., 1988. Interactive buckling in sandwich structures. *Proceedings of The Royal Society of London, Series A: Mathematical and Physical Sciences* 417 (1852), 155–177.
- Hutchinson, J., Evans, A., 2000. Mechanics of materials: top-down approaches to fracture. *Acta Materialia* 48 (1), 125–135.
- Jeelani, S., Carlsson, L., Saha, M., Islam, S., Mahfuz, H., 2005. Buckling of sandwich composites; effects of coreskin debonding and core density. *Applied Composite Materials* 12 (2), 73–91.
- Kim, S., Sridharan, S., 2005. Analytical study of bifurcation and nonlinear behavior of sandwich columns. *Journal of Engineering Mechanics* 131 (12), 1313–1321.
- Kwon, Y., Yoon, S., 1997. Compressive failure of carbon-foam sandwich composites with holes and/or partial delamination. *Composite Structures* 38 (1–4), 573–580.
- Legarth, B.N., 2004a. Fracture and damage with plastic anisotropy. Ph.D. Thesis, DCAMM, Report No. S91, Technical University of Denmark.
- Legarth, B., 2004b. Unit cell debonding analyses for arbitrary orientation of plastic anisotropy. *International Journal of Solids and Structures* 41 (26), 7267–7285.
- Li, S., Thouless, M., Waas, A., Schroeder, J., Zavattieri, P., 2005. Use of a cohesive-zone model to analyze the fracture of a fiber-reinforced polymer-matrix composite. *Composites Science and Technology* 65 (3–4), 537–549.

- Needleman, A., 1987. A continuum model for void nucleation by inclusion debonding. *Transactions of the ASME. Journal of Applied Mechanics* 54 (3), 525–531.
- Østergaard, R., Sørensen, B., Nødsted, P.B., 2006. Interface fracture toughness of sandwich structured loaded under mixed mode loading. *Journal of Sandwich Structure and Materials* 47 (6), 813–824.
- Prasad, S., Carlsson, L., 1994. Debonding and crack kinking in foam core sandwich beams-i. analysis of fracture specimens. *Engineering Fracture Mechanics* 47 (6), 813–824.
- Schellekens, J., De Borst, R., 1993. On the numerical integrations of interface elements. *International Journal for Numerical Methods in Engineering* 36 (1), 43–66.
- Somers, M., Weller, T., Abramovich, H., 1992. Buckling and postbuckling behavior of delaminated sandwich beams. *Composite Structures* 21 (4), 211–232.
- Thomsen, O.T., 2006. Polymer composites materials for wind power turbines. In: *Proceedings of the 27th Risø International Symposium on Materials Science*. Risø, Danish National Laboratory, pp. 97–114.
- Tvergaard, V., 1976. Effect of thickness inhomogeneities in internally pressurized elastic–plastic spherical shells. *Journal of the Mechanics and Physics of Solids* 24 (5), 291–304.
- Tvergaard, V., 1990. Effect of fibre debonding in a whisker-reinforced metal. *Materials Science and Engineering A: Structural Materials: Properties, Microstructure and Processing* A125 (2), 203–213.
- Tvergaard, V., Hutchinson, J., 1992. The relation between crack growth resistance and fracture process parameters in elastic–plastic solids. *Journal of the Mechanics and Physics of Solids* 40 (6), 1377–1397.
- Tvergaard, V., Hutchinson, J., 1993. The influence of plasticity on mixed mode interface toughness. *Journal of the Mechanics and Physics of Solids* 41 (6), 1119–1135.
- Vadakke, V., Carlsson, L., 2004. Experimental investigation of compression failure of sandwich specimens with face/core debond. *Composites Part B: Engineering* 35 (6–8), 583–590.
- Van Der Neut, A., 1973. The sensitivity of thin-walled compression members to column axis imperfection. *International Journal of Solids and Structures* 9 (8), 999–1011.
- Wadee, M.A., 2002. Localized buckling in sandwich struts with pre-existing delaminations and geometrical imperfections. *Journal of the Mechanics and Physics of Solids* 50 (8), 1767–1787.
- Wadee, M.A., Blackmore, A., 2001. Delamination from localized instabilities in compression sandwich panels. *Journal of the Mechanics and Physics of Solids* 49 (6), 1281–1299.
- Zenkert, D., Shipsha, A., 2005. Compression-after-impact strength of sandwich panels with core crushing damage. *Applied Composite Materials* 12 (3–4), 149–164.
- Zenkert, D., 1995. *An Introduction to Sandwich Construction*. Engineering Materials Advisory Services Ltd., London.